J. Appl. Numer. Optim. 8 (2026), No. 2, pp. 181-200
Available online at http://jano.biemdas.com
https://doi.org/10.23952/jano.8.2026.2.02

A PRECONDITIONED DESCENT ALGORITHM FOR A CLASS OF OPTIMIZATION PROBLEMS WITH THE $p(x)$-LAPLACIAN OPERATOR

SERGIO GONZÁLEZ-ANDRADE[1,2,*], MARÍA DE LOS ÁNGELES SILVA[1]

[1]*MODEMAT Research Center on Mathematical Modeling and Optimization, Quito, Ecuador*
[2]*Department of Mathematics, Escuela Politécnica Nacional, Ladrón de Guevara E11-253, Quito, Ecuador*

Abstract. In this paper, we are concerned with an optimization problem involving the $p(x)$-Laplacian operator, which serves as a model for a broader class of variational problems. We begin with a brief introduction to variable exponent spaces and study the well-posedness of the problem in a suitable functional framework, assuming that its exponent is log-Hölder continuous. For the numerical solution, we propose a preconditioned descent algorithm based on a "frozen exponent" strategy in finite-dimensional settings. We apply the method to two representative cases: the Poisson equation and a denoising-type problem. In both situations, numerical experiments are carried out to highlight the strengths of the proposed approach. Our main interest is to investigate the performance and practical potential of this class of preconditioned descent algorithms in solving nonlinear variational problems involving variable exponent operators.

Keywords. Denoising; Finite elements; $p(x)$-Laplacian operator; Poisson equation; Variable exponent spaces.

2020 Mathematics Subject Classification. 76M30, 65M60.

1. INTRODUCTION

This paper is concerned with the computational solution of the following optimization problem

$$\min_{u\in V^{p(\cdot)}(\Omega)} J(u) := \int_\Omega \frac{1}{p(x)}|\nabla u|^{p(x)}dx + \Xi_f(u), \tag{1.1}$$

where $\Omega \subset \mathbb{R}^N$, $N = 2,3$, is an open and bounded set, with regular boundary $\partial\Omega$. The space $V^{p(\cdot)}(\Omega)$ is a suitable variable-exponent function space. The operator $\Xi_f(u)$ incorporates information from the given data $f \in L^2(\Omega)$ and is assumed to be convex, differentiable, coercive and bounded from below in $L^2(\Omega)$. Finally, $p : \Omega \to (1,\infty)$ is a measurable function satisfying $1 < p(x) \leq 2$.

The $p(x)$-Laplacian operator is a functional extension of the classical Laplacian (when $p(x) \equiv 2$), and the p-Laplacian (when $p(x) \equiv p$, $1 < p < \infty$). The interest in this operator has become relevant in the recent years due to its applications in several models related to image processing and electrorheological fluids (see, e.g., [3, 8, 19]).

*Corresponding author.
E-mail address: sergio.gonzalez@epn.edu.ec (S. González-Andrade).
Received 11 June 2025; Accepted 27 December 2025; Published online 1 May 2026.

In order to discuss the theoretical properties of these problems, several authors have focused on the development of variable exponent function spaces and provided a solid background for the study of existence, uniqueness and regularity of solutions. In this regard, we start by citing [12], which we consider to be the best textbook to understand variable exponent spaces and their main features. In [2], the authors analyse the existence of solutions for the elliptic $p(x)$-Laplacian problem, considering diverse boundary conditions. In [17], the author analyses the existence of solutions for the Dirichlet $p(x)$-Laplacian problem from variational and topological perspectives. In [5], the authors consider the elliptic nonlinear $p(x)$-Laplacian problem and provide several regularity estimates considering specific hypothesis on both the variable exponent p and the associated nonlinearities. It is remarkable the work developed in [1], where the parabolic $p(x)$-Laplacian problem is considered and, furthermore, a class of amalgam spaces is introduced, giving a suitable framework for problems combining functions in variable exponent spaces and usual function spaces.

Regarding the numerical approach to $p(x)$-Laplacian problems, we mention [4], where the authors discuss in detail the finite element discretization of a vector elliptic $p(x)$-Laplacian problem, and introduce the idea of "frozen exponents", which follows from a local approximation of the variable exponent at each triangle of the FEM mesh. The authors obtain optimal approximation estimators for the discretized and the "frozen" problems. However, they do not perform computational experiments in this paper. In [10], the authors also discuss the finite element discretization of the elliptic $p(x)$-Laplacian equation and study the order of convergence for this approximation, providing optimal estimators and computational experiments. Further, in [9], the same authors discuss a discontinuous Galerkin discretization for a similar problem as the one we consider in this paper. They develop a detailed analysis of the approximation and perform one computational experiment for a one dimensional problem.

Considering a computational perspective, we refer to [6], where the authors propose an algorithm based on the BFGS method applied to the energy functional associated to the elliptic $p(x)$-Laplacian equation. Here, they carry out several numerical experiments and build benchmark examples for the elliptic Dirichlet problem. In [7], the same authors develop an algorithm based on the inverse power method to compute eigenvalues associated to the $p(x)$-Laplacian operator. They also provide several numerical experiments in diverse geometries.

When discussing the class of problems which are the main concern of this paper, we must start with [8]. In this contribution, the authors introduce a model for image restoration based on a functional involving a variable exponent. They propose the model and develop a detailed theoretical analysis. Further, they propose a computational approach by solving the Euler-Lagrange equations associated to the optimization problem. In [3], the authors extend the model proposed in [8] by considering a more general term for the fidelity term taking a L^q norm instead of a L^2 norm. Also, they develop computational experiments by a similar approach applied to the Euler-Lagrange equations.

In this paper, we study the well-posedness of problem (1.1) in a suitable variable exponent space, which provides an appropriate framework to analyze problems involving both local and nonlocal behaviors. To this end, we adapt techniques from the direct method in the calculus of variations to a functional defined over a space constructed following the ideas in [1]. The log-Hölder continuity of the exponent p ensures the viability of this approach, allowing us to work

with functionals that include terms in variable exponent spaces as well as terms in classical L^2 spaces.

Regarding the computational approximation, we take the discretize-then-optimize approach to the problem. Thus, we start by proposing a finite element approximation for (1.1), and we develop a preconditioned descent algorithm, based on the construction of preconditioned descent directions, for the discretized objective functional. The main idea is to extend the variational and optimization techniques from [13] to the $p(x)$-Laplacian structure. With this aim, we adapt the "frozen exponent" approach from [4] to the present case. Once we have the "frozen problem" defined and analysed, we propose to compute the preconditioned descent directions by solving, iteratively, a variational equation involving a local approximation for the $p(x)$-Laplacian operator. Further, we are able to construct a modular, which can be seen as a weighted norm in the finite element space, to prove that the preconditioned descent directions for the "frozen" problems are indeed descent directions for the objective functional. The main advantage of the proposed method is that each iteration only demands the solution of one linear system of equations involving a weighted system matrix. This fact makes the total computational cost low, especially when compared with other algorithmic tools like quasi-Newton algorithms or the numerical solution of complex systems of PDEs.

The rest of the paper is organized as follows. In the next section we present the variable exponent function spaces and their main properties. In Section 3, we state the optimization problem and discuss its well-posedness in a suitable space, by using the direct method of calculus of variations. Section 4 is devoted to the development of the preconditioned descent algorithm. Here, we propose the finite element discretization for the problem and discuss the "frozen exponent" approach. Next, we write and briefly analyse the algorithm and its main features. Mainly, we prove that the solutions of the variational equation involving the approximation of the $p(x)$-Laplacian operator are in fact descent directions for the objective functional. In Section 5, we carry out three detailed numerical experiments to show the performance of the algorithm. First, we apply our method to the Dirichlet elliptic $p(x)$-Laplacian equation to validate the approach. Then, we show two experiments in two dimensional domains to show the ability of the algorithm to recover smooth approximations from noisy functions. Finally, the last section, Section 6, is devoted to the conclusions and research perspectives.

2. Spaces with Variable Exponent

In this section, we introduce the function spaces with variable exponent which we use in the forthcoming analysis, and show several properties of them. Let $\Omega \subset \mathbb{R}^N$, $N = 2,3$, be an open and bounded set, and let $p : \Omega \to (1,\infty]$ be a measurable function, which will be called a variable exponent on Ω. For such a function p, we define the following values

$$p^- := p^-_\Omega := \operatorname*{ess\,inf}_{y\in\Omega} p(y) \text{ and } p^+ := p^+_\Omega := \operatorname*{ess\,sup}_{y\in\Omega} p(y).$$

If $p^+ < \infty$, p is said to be a bounded variable exponent.

Definition 2.1. Let $\Omega \subset \mathbb{R}^N$ be an open and bounded set and let p be a variable exponent. We define the Lebesgue space with variable exponent $L^{p(\cdot)}(\Omega)$ to be the space of measurable functions for which the modular

$$\rho_{p(\cdot)}(u) := \int_\Omega |u(x)|^{p(x)}\, dx$$

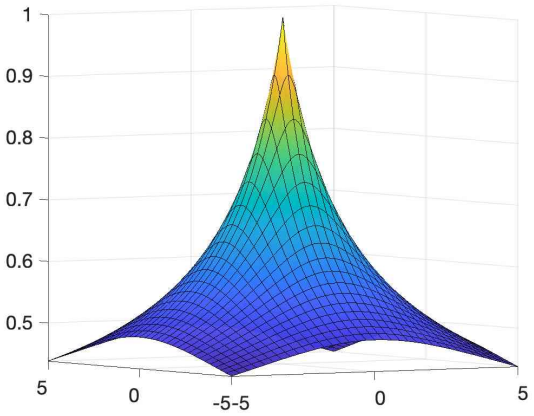

FIGURE 1. Example of a globally log-Hölder continuous function: $p(x) = 1/(\log(e+|x|))$.

is finite. Further, we equip this space with the following Luxemburg norm

$$\|u\|_{L^{p(\cdot)}(\Omega)} = \inf\{\zeta > 0 : \rho_{p(\cdot)}(u/\zeta) \leq 1\}.$$

Proposition 2.1. *Let $p : \Omega \to [1,\infty)$ be a variable exponent. Then, for all $w \in L^{p(\cdot)}(\Omega)$,*

$$\sigma^-\left(\|w\|_{p(\cdot)}\right) \leq \int_\Omega |w(x)|^{p(x)} dx \leq \sigma^+\left(\|w\|_{p(\cdot)}\right),$$

where, for $s \geq 0$, $\sigma^-(s) := \min\{s^{p^-}, s^{p^+}\}$ and $\sigma^+(s) := \max\{s^{p^-}, s^{p^+}\}$.

Proof. For a proof, we refer the reader to [1, Prop. 2.1] and the references therein. □

Definition 2.2. Let $\Omega \subset \mathbb{R}^N$ be an open and bounded set, and let p be a variable exponent. We define the Sobolev space with variable exponent $W^{1,p(\cdot)}(\Omega)$ as follows

$$W^{1,p(\cdot)}(\Omega) := \left\{ u \in L^{p(\cdot)}(\Omega) : \frac{\partial u}{\partial x_i} \in L^{p(\cdot)}(\Omega), \text{ for all } i = 1,2,\ldots,N \right\}.$$

This space is equipped with the norm

$$\|u\|_{W^{1,p(\cdot)}(\Omega)} := \left(\|u\|^2_{L^{p(\cdot)}(\Omega)} + \|\nabla u\|^2_{\mathbf{L}^{p(\cdot)}(\Omega)} \right)^{1/2}.$$

Remark 2.1. With the definitions above, it is established in [12, Sec. 3.4 and Sec 8.1] that $L^{p(\cdot)}(\Omega)$ and $W^{1,p(\cdot)}(\Omega)$ are separable. Furthermore, if $1 < p^-$ and $p^+ < \infty$, then $L^{p(\cdot)}(\Omega)$ and $W^{1,p(\cdot)}(\Omega)$ are uniformly convex Banach spaces, and consequently, these spaces are reflexive.

Let $p : \Omega \to [0,\infty)$ be a variable exponent. p is said to be log-Hölder continuous if there exists a constant $A > 0$ such that

$$|p(x) - p(y)| \leq \frac{A}{\log(e + 1/|x-y|)}, \quad \text{for all } x, y \in \Omega. \tag{2.1}$$

This property implies that $p \in C(\overline{\Omega})$ and $p^+ < \infty$ (see [12, p. 100]). In Figure 1, we depict the function $p(x) = 1/(\log(e+|x|))$, which is globally log-Hölder continuous, with constant $A = 1$.

The space $W_0^{1,p(\cdot)}(\Omega)$ is defined as the closure of the following set

$$\{w \in W^{1,p(\cdot)}(\Omega) : u = u\chi_K, \text{for some compact set } K \subset \Omega\}$$

in the topology of $W^{1,p(\cdot)}(\Omega)$. However, if the variable exponent p satisfies (2.1), this space is equivalently defined as the closure of $C_0^\infty(\Omega)$ in $W^{1,p(\cdot)}(\Omega)$. This space is usually characterized as the Sobolev space with zero boundary values (see [12, Sec. 8]).

Hereafter, we use the space $W_0^{1,p(\cdot)}(\Omega)$ under the hypothesis that p is log-Hölder continuous. In this case, [12] guarantees that the following Poincaré inequality holds: there exists a constant $C \geq 0$ such that

$$\|u\|_{L^{p(\cdot)}(\Omega)} \leq C\|\nabla u\|_{\mathbf{L}^{p(\cdot)}(\Omega)}, \text{ for all } u \in W_0^{1,p(\cdot)}(\Omega).$$

Hence, we can equip the space $W_0^{1,p(\cdot)}(\Omega)$ with the following norm

$$\|u\|_{W_0^{1,p(\cdot)}(\Omega)} := \|\nabla u\|_{\mathbf{L}^{p(\cdot)}(\Omega)},$$

which is known to be equivalent with $\|\cdot\|_{W^{1,p(\cdot)}(\Omega)}$. Furthermore, if we assume that the variable exponent p is log-Hölder continuous, that Ω is bounded with regular boundary $\partial\Omega$ and that $p^- \geq 2N/(N+2)$, [1, Prop. 2.2 and pp. 42] guarantees the existence of a constant $C \geq 0$ such that

$$\|u\|_{L^2(\Omega)} \leq C\|u\|_{W_0^{1,p(\cdot)}(\Omega)}, \text{ for all } u \in W_0^{1,p(\cdot)}(\Omega).$$

These inequalities suggest that the well-posedness of (1.1) could be analysed in the following space with a variable exponent

$$V_0^{p(\cdot)}(\Omega) := W_0^{1,p(\cdot)}(\Omega) \cap L^2(\Omega)$$

equipped with the norm

$$\|u\|_{V_0^{p(\cdot)}(\Omega)} := \left(\|u\|^2_{L^2(\Omega)} + \|\nabla u\|^2_{\mathbf{L}^{p(\cdot)}(\Omega)}\right)^{1/2}.$$

In fact, by folllowing [1, p. 42], and by assuming that $1 < p^-$ and $p^+ < \infty$, we can state that $V^{p(\cdot)}(\Omega)$ is a reflexive Banach space. Moreover, in [1, Prop. 2.4] it is established that, under the log-Hölder hypothesis on $p(\cdot)$, this space coincides with the so called amalgam space

$$X_0^{p(\cdot)}(\Omega) := \left\{u \in L^2(\Omega) : \frac{\partial u}{\partial x_i} \in L^{p(\cdot)}, \text{ for } i = 1, \ldots, N\right\}.$$

3. Well-posedness of the Optimization Problem

Once the variable exponent spaces are introduced and the appropriate functional setting for (1.1) is established, we recall the problem and focus on its well-posedness.

$$\min_{u \in V_0^{p(\cdot)}(\Omega)} J(u) := \int_\Omega \frac{1}{p(x)} |\nabla u|^{p(x)} dx + \Xi_f(u). \tag{3.1}$$

In what follows, we consider a general functional $\Xi_f(u)$, which is convex, differentiable and bounded from below on $L^2(\Omega)$.

Proposition 3.1. *Let p be a variable exponent such that $1 < p^- \leq p(x) \leq p^+ \leq 2$. Then, the functional J in (3.1) is bounded from below and weakly lower semicontinuous (w.l.s.c) in $V_0^{p(\cdot)}(\Omega)$.*

Proof. Let us start by noticing that Proposition 2.1 yields that there exists a constant C such that

$$\int_\Omega \frac{1}{p(x)}|\nabla u|^{p(x)}\,dx \geq \frac{1}{p^+}\sigma^-(||\nabla u||_{p(\cdot)})$$

which implies, together with the boundedness assumption on $\Xi_f(u)$, that J is bounded from below. Consequently, it is possible to conclude that there exists $\hat{u} \in V_0^{p(\cdot)}(\Omega)$ such that

$$J(\hat{u}) = \inf_{u \in V_0^{p(\cdot)}(\Omega)} J(u).$$

Next, in order to prove that $J(\cdot)$ is weakly lower semi continuous (w.l.s.c.) in $V_0^{p(\cdot)}(\Omega)$, we introduce the functional $\Psi : V_0^{p(\cdot)}(\Omega) \to \mathbb{R}$ as follows

$$\Psi(u) := \int_\Omega \frac{1}{p(x)}|\nabla u(x)|^{p(x)}dx.$$

We show that $\Psi(u)$ is a continuous functional in $V_0^{p(\cdot)}(\Omega)$. Indeed, let $\{u_k\} \subset V_0^{p(\cdot)}(\Omega)$ be a sequence such that $u_k \to u \in V_0^{p(\cdot)}(\Omega)$, as $k \to \infty$. Then, we have that

$$u_k \to u \text{ in } L^2(\Omega) \text{ and } \nabla u_k \to \nabla u \text{ in } L^{p(\cdot)}(\Omega).$$

On the other hand, we have that

$$\left|\frac{1}{p(x)}|\nabla u_k(x)|^{p(x)}\right| \leq \frac{1}{p^-}|\nabla u_k(x)|^{p(x)}, \text{ a.e. in } \Omega,$$

which implies by $\{\nabla u_k\} \in L^{p(\cdot)}(\Omega)$ that $\frac{1}{p^-}|\nabla u_k(x)|^{p(x)} \in L^1(\Omega)$. Thanks to the Lebesgue's dominated convergence theorem, we have that

$$\Psi(u_k) = \int_\Omega \frac{1}{p(x)}|\nabla u_k(x)|^{p(x)}dx \to \int_\Omega \frac{1}{p(x)}|\nabla u(x)|^{p(x)}dx = \Psi(u).$$

Convexity of Ψ in $V_0^{p(\cdot)}(\Omega)$ directly follows from the fact that the application $u \mapsto u^{p(x)}$ is known to be convex for $1 < p^{\leq} p(x) \leq p^+ \leq 2$ (see [12, Th. 3.4.9]).

Finally, since $\Xi_f(u)$ is assumed to be convex and differentiable in $L^2(\Omega)$, we can state that it is continuous in $V_0^{p(\cdot)}(\Omega)$. Hence, thanks to [20, Th. 2.12], we conclude that Ψ and Ξ_f are w.l.s.c. in $V_0^{p(\cdot)}(\Omega)$. Finally, thanks to [15, Sec. 1.2.2], we can state that $J(u) = \Psi(u) + \Xi_f(u)$ is a weakly lower semicontinuous functional in $V_0^{p(\cdot)}(\Omega)$. □

The Proposition above provides the basic elements to complete the existence proof by using the direct method of the calculus of variations. Based on this approach, we have the following existence and uniqueness result

Theorem 3.1. *Let p be a variable exponent such that $1 < p^- \leq p(x) \leq p^+ \leq 2$. Then, problem (3.1) has a unique solution $\bar{u} \in V_0^{p(\cdot)}(\Omega)$.*

Proof. We start by introducing a minimizing sequence $\{u_k\} \subset V_0^{p(\cdot)}(\Omega)$ such that

$$J(u_k) \to J(\hat{u}) = \inf_{u \in V_0^{p(\cdot)}(\Omega)} J(u), \text{ as } k \to \infty.$$

Next, let us show that $\{u_k\}_{n\in\mathbb{N}}$ is bounded in $V_0^{p(\cdot)}(\Omega)$. In fact, note that Proposition 2.1 implies that

$$J(u_k) \geq \frac{1}{p^+}\sigma^-(||\nabla u_k||_{p(\cdot)}) + \Xi_f(u_k). \tag{3.2}$$

On the other hand, we know that $||u||_{V_0^{p(\cdot)}(\Omega)} = (||u||^2_{L^2(\Omega)} + ||\nabla u||^2_{p(\cdot)})^{1/2}$. If $||u_k||_{V_0^{p(\cdot)}(\Omega)} \to +\infty$, it follows that $||u_k||^2_{L^2(\Omega)} \to +\infty$ and/or $||\nabla u_k||^2_{L^{p(\cdot)}(\Omega)} \to +\infty$. If $||u_k||_{V_0^{p(\cdot)}(\Omega)} \to +\infty$, (3.2) and the fact that Ξ is assumed to be coercive in $L^2(\Omega)$ imply that

$$\lim_{\|u_k\|_{V_0^{p(\cdot)}(\Omega)}\to\infty} J(u_k) = +\infty.$$

Therefore, we can conclude that J is a coercive functional in $V_0^{p(\cdot)}(\Omega)$, which implies that the minimizing sequence must be bounded. Further, since J is a w.l.s.c. and coercive functional, [15, Th. 1.5 and Th. 1.6] implies that (1.1) has a solution $\bar{u} \in V_0^{p(\cdot)}(\Omega)$. Finally, the uniqueness follows from the strict convexity of J. □

Remark 3.1. In this paper, we consider the following two representative problems:

- **The $p(x)$-Poisson problem:** in this case, the functional Ξ_f is defined by

$$\Xi_f(u) := -\int_\Omega f\,u\,dx,$$

  where f is a given function in $L^2(\Omega)$.
- **A denoising-type problem:** here, the functional Ξ_f is given by

$$\Xi_f(u) := \frac{\lambda}{2}\int_\Omega |u-f|^2\,dx,$$

  where $\lambda \geq 0$ is a given constant and f is given in $L^2(\Omega)$.

In both cases, it is possible to show that $\Xi_f(u)$ is convex, differentiable, bounded from below, and coercive in $L^2(\Omega)$. Therefore, the theoretical results established above apply.

4. A Preconditioned Deepest Descent Algorithm

We analyze the numerical solution of problem (3.1) by a discretize-then-optimize approach. Thus, we propose a finite element discretization for the problem. Then, let $\mathscr{T}^h$ be a regular triangulation, in the sense of Ciarlet, of Ω. Next, let Ω^h be a polygonal approximation of Ω, given by $\Omega^h := \cup_{\tau\in\mathscr{T}^h}\overline{\tau}$, where all the open disjoint regular triangles have maximum diameter bounded by h. Further, for any two triangles, their closures are either disjoint or have a common vertex or a common side. Finally, let $\{P_j\}_{j=1,\dots,n}$, $n\in\mathbb{N}$, be the vertices associated with the triangulation $\mathscr{T}^h$. Hereafter, we assume that $P_j \in \partial\Omega^h$ implies that $P_j \in \partial\Omega$ and that $\Omega^h \subset \Omega$.

On the other hand, since $N = 2$ and p is assumed to be log-Hölder continuous, by following [4], we define the finite dimensional space $V_0^h \subset V_0^{p(\cdot)}(\Omega)$, as follows

$$V_0^h := V_h \cap V_0^{p(\cdot)}(\Omega), \text{ with } V_h := \{v \in C(\Omega^h) : v|_\tau \in \mathbb{P}_1,\ \forall \tau \in \mathscr{T}^h\}.$$

Here, $\mathbb{P}_1$ is the space of polynomials with degree at most 1. In this paper we will only consider first order approximation, since the solutions of the p-Laplacian type problems usually exhibit limited higher order regularity (see [6, 16] and the references therein).

Considering the discussion above, we introduce the discretized optimization problem as follows

$$\min_{u_h \in V_0^h} J_h(u_h) := \int_\Omega \frac{1}{p(x)} |\nabla u_h|^{p(x)} dx + \Xi_f(u_h). \tag{4.1}$$

Since p is a log-Hölder continuous function, considering the results in [4], it is possible to state that the discretized problem has a unique solution. Indeed, the direct application of a similar argumentation as the one used in Section 3, considering that V_0^h is a closed subspace of $V_0^{p(\cdot)}(\Omega)$, yields the existence of a unique solution for the discretized problem (4.1).

4.1. **Frozen exponents.** We propose to use the technique of frozen exponents developed in [4]. The main idea is to propose a local approximation of the variable exponent and use this approximation in the discretized functional. To this end, we use a simple weighting operator to obtain the value of the function p in the gravity center x_τ of each triangle $\tau \in \mathscr{T}^h$, obtaining the following

$$p_{\mathscr{T}}(x) := \sum_{\tau \in \mathscr{T}^h} p(x_\tau) \chi_\tau(x).$$

Once we have this local approximation for the variable exponent, we focus on the following problem

$$\min_{u_h \in V_0^h} J_{h,\mathscr{T}}(u_h) := \int_\Omega \sum_{\tau \in \mathscr{T}^h} \chi_\tau(x) \frac{1}{p(x_\tau)} |\nabla u_h|^{p(x_\tau)} dx + \Xi_f(u_h). \tag{4.2}$$

Next, according to [4, Rem. 4.7], the norms $\|\cdot\|_{p(\cdot)}$ and $\|\cdot\|_{p_{\mathscr{T}}(\cdot)}$ are equivalent on any finite element space, and thus also on V_0^h. This result guarantees the existence of a unique solution to problem (4.2). Furthermore, by following [4, Th. 4.9] and assuming that $p \in C^{0,\alpha}(\overline{\Omega})$ with $p^- > 1$, one can obtain the following estimator

$$\|J'_{h,\mathscr{T}}(u_h) - J'_{h,\mathscr{T}}(\overline{u}_h)\|_{2,h} \leq C h^\alpha, \tag{4.3}$$

where $\overline{u}_h$ denotes the finite element solution of problem (4.1). The discrete derivative reads

$$J'_{h,\mathscr{T}}(u_h) v_h := \int_\Omega \sum_{\tau \in \mathscr{T}^h} \chi_\tau(x) \, |\nabla u_h|^{p(x_\tau)-2} \nabla u_h \cdot \nabla v_h \, dx + \Xi'_f(u_h) v_h, \tag{4.4}$$

and the discrete L^2-type norm is defined as

$$\|v_h\|_{2,h}^2 := \sum_{\tau \in \mathscr{T}^h} \int_\tau |v_h(x_\tau)|^2 \, dx. \tag{4.5}$$

The term $\Xi'_f(u_h) v_h$ corresponds to the derivative of the data-fidelity contribution.

We shall assume that these theoretical properties hold true, and we now proceed to present the computational approach for problem (4.2).

4.2. **A preconditioned descent direction.** The computational approach that we propose for problem (4.2) is based on the construction of descent directions by solving, iteratively, the following variational equation

$$\int_\Omega \sum_{\tau \in \mathscr{T}^h} \chi_\tau(x) (\varepsilon + |\nabla u_h|)^{p(x_\tau)-2} \nabla w_h \cdot \nabla v_h \, dx = -J'_{h,\mathscr{T}}(u_h) v_h, \text{ for all } v_h \in V_0^h. \tag{4.6}$$

We state that the solution w_h is a descent direction for the functional $J_{h,\mathscr{T}}(u_h)$. In fact, we start this discussion by introducing the following expression in V_0^h

$$\rho_u^h(w^h) := \int_\Omega \left(\sum_{\tau\in\mathscr{T}^h} \chi_\tau(x)(\varepsilon + |\nabla u_h|)^{p(x_\tau)-2} \right) |\nabla w_h|^2 \, dx. \tag{4.7}$$

It is not difficult to prove that $\rho_u^h(w^h)$ is a modular in V_0^h, according to [12, Def. 2.1.1]. Particularly, we have that

$$\rho_u^h(w_h) > 0, \text{ for all } w_h \in V_0^h, \text{ and } \rho_u^h(w_h) = 0, \text{ iff } w_h = 0.$$

Therefore, if we take $v_h = w_h$ in (4.6), we have that

$$-J'_{h,\mathscr{T}}(u_h)w_h = \int_\Omega \left(\sum_{\tau\in\mathscr{T}^h} \chi_\tau(x)(\varepsilon + |\nabla u_h|)^{p(x_\tau)-2} \right) |\nabla w_h|^2 \, dx = \rho_u^h(w_h) > 0,$$

which yields that w_h is, indeed, a descent direction for $J_{h,\mathscr{T}}(u_h)$.

Remark 4.1. Existence and uniqueness of solutions for the equation (4.6) can be analyzed by using the ideas in [13] or [16]. This implies either the construction of a Hilbert subspace in V_0^h in which the modular $\rho_u^h(w_h)$ acts as a induced norm, or the analysis of the modular as a weighted norm in V_0^h. This analysis, however, is in our consideration out of the scope of the present work. We will return to this discussion in future contributions focused on the development of mesh independent algorithms for problems involving the $p(x)$-Laplacian.

Summarizing, we propose the following preconditioned deepest descent algorithm for the problems under study

Algorithm 4.1. (Preconditioned Descent Algorithm - PDA)
Define the parameters ε, λ and tol. Further, set f, initialize $u_h^0 \in V_0^h$ and set $k = 0$.
For $k = 1, 2, \ldots$

(1) If $\frac{\|J'_{h,\mathscr{T}}(u_h^k)\|_{2,h}}{\|J'_{h,\mathscr{T}}(u_h^0)\|_{2,h}} \leq tol$, STOP.
(2) Find a descent direction $w_h^k \in V_0^h$ by solving

$$\int_\Omega \sum_{\tau\in\mathscr{T}^h} \chi_\tau(x)(\varepsilon + |\nabla u_h^k|)^{p(x_\tau)-2} \nabla w_h^k \cdot \nabla v_h \, dx = -J'_{h,\mathscr{T}}(u_h^k)v_h, \text{ for all } v_h \in V_0^h. \tag{4.8}$$

(3) Perform an efficient line search technique to obtain the step length $\alpha_k > 0$.
(4) Update $u_h^{k+1} := u_h^k + \alpha_k w_h^k \in V_0^h$ and set $k = k+1$.

Remark 4.2. The convergence of the Algorithm (PDA) follows by standard arguments. In fact, let us point out that $J_{h,\mathscr{T}}(u_h)$ is a convex and differentiable functional on V_0^h and that w_h is a descent direction. Thus, if we consider a line search algorithm satisfying the Wolfe-Powell conditions, the global convergence of the algorithm is guaranteed (See [18]). We propose to use a backtracking algorithm based on interpolation developed in [11], which will be presented in the following section.

5. Numerical Results

This section presents numerical experiments to evaluate the performance of the proposed preconditioned descent algorithm. We consider two classes of problems: the $p(x)$-Poisson equation, which serves as a validation benchmark, and a denoising-type variational problem that demonstrates the method's applicability to image restoration tasks. The discussion covers the experimental setup and implementation aspects, such as the polynomial interpolation-based line search.

We start by defining the stopping criterion for Algorithm 4.1 (PDA), which terminates when the gradient norm ratio

$$\frac{\|J'_{h,\mathscr{T}}(u_h^k)\|_{2,h}}{\|J'_{h,\mathscr{T}}(u_h^0)\|_{2,h}}$$

falls below a tolerance factor of 10^{-6} or 10^{-5}, depending on the experiment. Such tolerance factors are commonly employed in descent algorithms and ensure a good balance between accuracy and computational cost in similar contexts (see [13]).

An important feature of Algorithm 4.1 (PDA) is its computational efficiency, achieved by solving only one linear system per iteration. Specifically, at each iteration k, the descent direction w_h^k is obtained by solving the system

$$A_{\varepsilon,u}^h w_h^k = \eta_h,$$

where $A_{\varepsilon,u}^h$ denotes the finite element matrix associated with the bilinear form

$$\int_\Omega \sum_{\tau\in\mathscr{T}^h} \chi_\tau(x)(\varepsilon+|\nabla u_h^k|)^{p(x_\tau)-2}\nabla w_h^k\cdot\nabla v_h\,dx,$$

and η_h is the load vector corresponding to the linear form $-J'_{h,\mathscr{T}}(u_h^k)v_h$. The matrix $A_{\varepsilon,u}^h$ is symmetric and positive definite, and it depends exclusively on the current iterate u_h^k, making it invariant with respect to the unknown w_h^k. This structure allows the use of efficient solvers and ensures that the computational cost per iteration remains low. In all numerical experiments, we used a fixed value of $\varepsilon = 10^{-6}$ for the regularization parameter.

For the step size selection in step 3 of Algorithm 4.1 (PDA), we employ a backtracking line search based on polynomial interpolation. This approach, detailed in Algorithm 5.1, constructs successive quadratic and cubic models of the objective function along the search direction to determine a step size that ensures sufficient decrease while minimizing functional evaluations.

Algorithm 5.1. (Backtracking line search algorithm)
Let $\sigma\in(0,\frac{1}{2})$ and $\tau_0 = 1$.

(1) Decide whether $J_{h,\mathscr{T}}(u^k+\tau_k w_h^k)\le J_{h,\mathscr{T}}(u^k)+\sigma J'_{h,\mathscr{T}}(u^k)(\tau_k w_h^k)$ holds. If so, STOP and let $\tau_k=\tau_0$. Otherwise:
(2) Decide whether the step length is too small. If so, STOP and terminate algorithm: routine failed to locate u^{k+1} sufficiently distinct from u^k. Otherwise:
(3) Decrease τ by a factor between 0.1 and 0.5 as follows:
  (a) On the first backtrack: let $\tau_k := \tilde{\tau}_2 = \arg\min m_2(\tau)$, but constraint the new τ_k to be greater than 0.1.
  (b) On all the subsequent backtracks: set $\tau_k := \tilde{\tau}_3 = \arg\min m_3(\tau)$, but constraint the new τ_k to be in $[0.1\tau_p, 0.5\tau_p]$.

(4) Return to step 1.

The polynomial models $m_2(\tau)$ and $m_3(\tau)$ approximate the scalar function $\varphi_k(\tau) := J_{h,\mathscr{T}}(u^k + \tau w_h^k)$ along the search direction. The quadratic model $m_2(\tau)$ is defined as

$$m_2(\tau) := \left(\varphi_k(1) - \varphi_k(0) - \varphi_k'(0)\right)\tau^2 + \varphi_k'(0)\tau + \varphi_k(0),$$

while the cubic model m_3 is given by

$$m_3(\tau) = c\tau^3 + d\tau^2 + \varphi_k'(0)\tau + \varphi_k(0),$$

with coefficients determined by

$$\begin{pmatrix} c \\ d \end{pmatrix} = \frac{1}{\tau_{\mathrm{p}} - \tau_{2\mathrm{p}}} \begin{pmatrix} \frac{1}{\tau_{\mathrm{p}}^2} & -\frac{1}{\tau_{2\mathrm{p}}^2} \\ -\frac{\tau_{2\mathrm{p}}}{\tau_{\mathrm{p}}^2} & \frac{\tau_{\mathrm{p}}}{\tau_{2\mathrm{p}}^2} \end{pmatrix} \begin{pmatrix} \varphi_k(\tau_{\mathrm{p}}) - \varphi_k(0) - \varphi_k'(0)\tau_{\mathrm{p}} \\ \varphi_k(\tau_{2\mathrm{p}}) - \varphi_k(0) - \varphi_k'(0)\tau_{2\mathrm{p}} \end{pmatrix}.$$

Here τ_p and τ_{2p} denote the two most recent previous values of τ_k.

This interpolation-based backtracking strategy, originally introduced in [11], was adapted for preconditioned descent methods applied to similar problems in [13, 14]. A key feature of this technique is that it satisfies the Wolfe-Powell conditions and ensures global convergence of Algorithm 4.1 (PDA). In practice, the method typically converges within 2-3 backtracking iterations, maintaining computational efficiency while guaranteeing sufficient decrease. For the complete convergence analysis and implementation details, see [11, Section 6.3.2].

5.1. **The $p(x)$-Poisson equation: algorithm validation.** In this section, we consider the $p(x)$-Laplacian elliptic problem

$$\begin{cases} -\mathrm{div}(|\nabla u(x)|^{p(x)-2}\nabla u(x)) = f(x) & \text{in } \Omega \\ u(x) = 0 & \text{on } \partial\Omega, \end{cases} \tag{5.1}$$

where $\Omega \subset \mathbb{R}^N$ is an open bounded domain with regular boundary. For validation against the benchmark in [6], we take $\Omega = B_1(0,0)$ with $f = 1$ and the following variable exponent

$$p(x) = \begin{cases} p^+ & \text{if } x < -0.01 \\ p^- + (p^- - p^+)\frac{x-0.01}{0.02} & \text{if } |x| \le 0.01 \\ p^- & \text{if } x > 0.01, \end{cases}$$

with $p^+ = 4$ and $p^- = 1.1$.

It is well known that the solution to this problem is characterized as the minimizer of the following variational problem [6]

$$\min_{u_h \in V_0^h} J(u_h) := \int_\Omega \frac{1}{p(x)}|\nabla u_h|^{p(x)}\,dx - \int_\Omega f u_h\,dx,$$

which corresponds to problem (4.2) with $\Xi_f(u_h) = -\int_\Omega f u_h, dx$. Therefore, we approximate the solutions of (5.1) with the Algorithm 4.1 (PDA). We employ a uniform mesh with $h = 0.0086$ and set the tolerance to 7.5×10^{-5}.

Figure 2 shows the computed solution u_h, which exhibits excellent agreement with the reference solution in [6, Fig. 3]. Figure 3 displays the convergence behavior, where the left panel shows the rapid decrease of the relative gradient norm, indicating convergence to a stationary

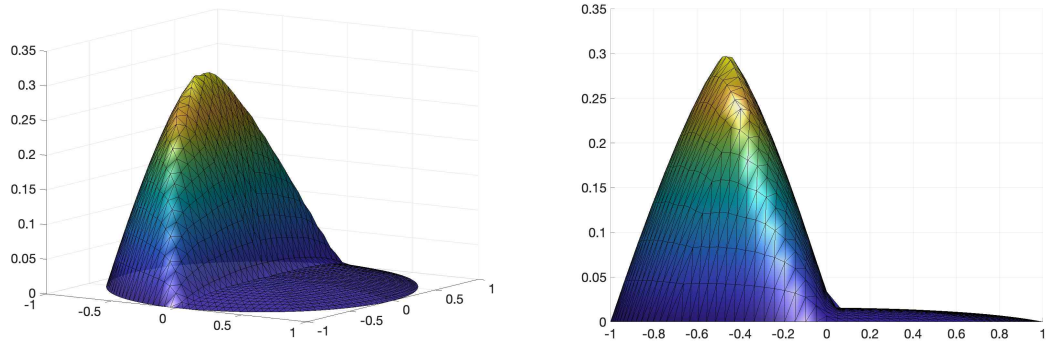

FIGURE 2. Computed solution of the benchmark $p(x)$-Poisson problem

point. The right panel confirms the monotonic decrease of the objective functional, which stabilizes at approximately -0.1404. The final iterations of the convergence history for $h = 0.0086$ are detailed in Table 1, showing the evolution of the gradient norm and objective functional as the algorithm approaches the stopping criterion.

# it.	$\frac{\|J'_{h,\mathscr{T}}(u_h^k)\|_{2,h}}{\|J'_{h,\mathscr{T}}(u_h^0)\|_{2,h}}$	$J_{h,\mathscr{T}}(u_h^k)$
13	9.5988e-4	-0.1400
14	7.4323e-4	-0.1404
15	8.6318e-4	-0.1404
16	6.9567e-4	-0.1404
17	5.6333e-6	-0.1404

TABLE 1. Convergence history for the benchmark $p(x)$-Poisson problem.

To evaluate the sensitivity of the proposed algorithm with respect to mesh refinement, we tested its performance over several discretization levels. Table 2 summarizes the results obtained for different mesh sizes h, reporting the number of iterations required for convergence, the final value of the stopping criterion and the corresponding objective functional value $J_{h,\mathscr{T}}(u_h^k)$. Figure 4 depicts the evolution of the residual along the iterations for each mesh size h. Although minor variations can be observed among the different discretizations, the overall convergence pattern is consistent and clearly exhibits a monotone decay. This robustness across meshes suggests that the method is not significantly affected by the discretization level, motivating a more detailed study of possible mesh-independence properties in future work.

5.2. **A denoising-type problem.** This section examines the application of Algorithm 4.1 (PDA) to a denoising-type problem, formulated as the variational problem (4.2) with the fidelity term $\Xi_f(u) := \frac{\lambda}{2}\int_\Omega |u-f|^2 dx$. The data $f = u_e + \xi$ represents a noisy version of the ground truth function u_e, corrupted by additive Gaussian noise ξ with zero mean and standard deviation proportional to the specified noise level.

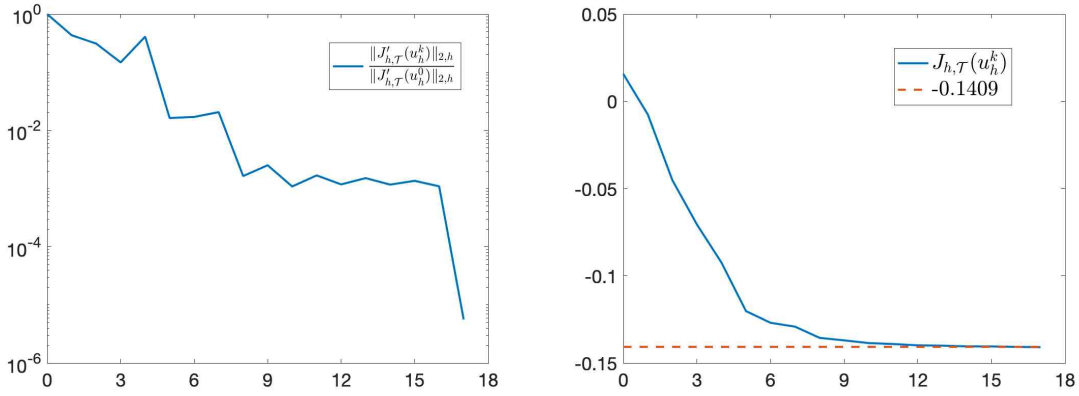

FIGURE 3. Algorithm convergence: gradient norm ratio (left) and objective function (right) for the $p(x)$-Poisson problem.

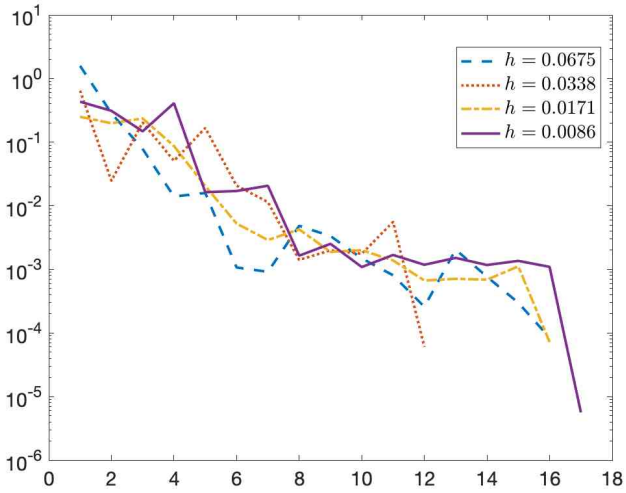

FIGURE 4. Gradient norm evolution across mesh sizes h for the $p(x)$-Poisson benchmark.

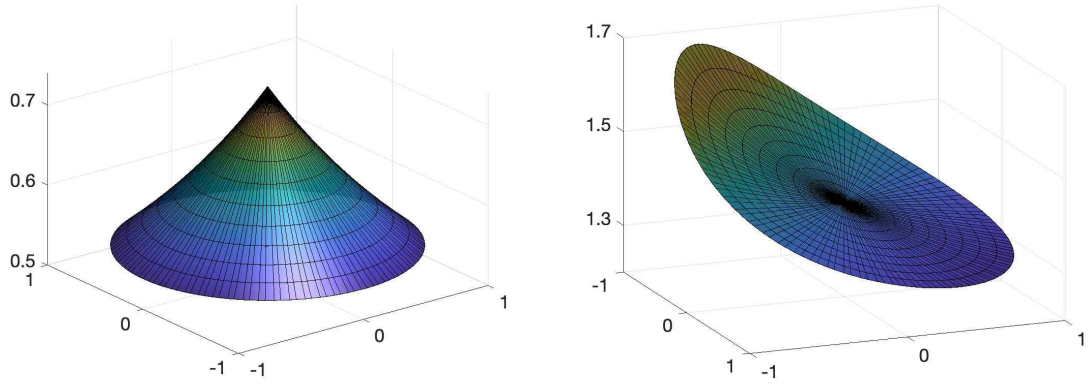

FIGURE 5. Variable exponents p_1 (left) and p_2 (right)

h	# it.	$\frac{\|J'_{h,\mathscr{T}}(u_h^k)\|_{2,h}}{\|J'_{h,\mathscr{T}}(u_h^0)\|_{2,h}}$	$J_{h,\mathscr{T}}(u_h^k)$
0.0675	17	1.5698e-6	-0.1607
0.0338	12	6.0577e-5	-0.1465
0.0171	16	7.1957e-5	-0.1425
0.0086	17	5.6333e-6	-0.1404

TABLE 2. Mesh sensitivity analysis: algorithm performance for the $p(x)$-Poisson benchmark across different mesh sizes h.

For all experiments, we take $\Omega = B_1(0,0)$ and define the exact function u_e as the solution of the boundary value problem

$$\begin{cases} -\Delta u &= \frac{\sqrt{\beta}}{\alpha}\exp\left(\frac{\alpha(x_1+x_2+\beta)+\beta}{\beta}\right), & \text{in } \Omega \\ u &= 0, & \text{on } \partial\Omega, \end{cases}$$

with parameters $\alpha = 1.5$ and $\beta = 1.0$. The function u_e is computed numerically using the same finite element discretization as the denoising problem to ensure consistent error evaluation.

We evaluate the reconstruction quality using the relative L^2 error

$$err_u := \frac{\|u_h - u_e\|_{2,h}}{\|u_e\|_{2,h}}.$$

The performance of Algorithm 4.1 (PDA) is investigated using two variable exponents (Figure 5)

$$p_1((x_1,x_2)) := \frac{2}{\log(e+\sqrt{x_1^2+x_2^2})} \text{ and } p_2((x_1,x_2)) := 1+\left(\frac{3}{4}(x_1+x_2)+2.5\right)^{-1}.$$

Both exponents are log-Hölder continuous and satisfy $1 < p(x) < 2$ throughout Ω.

5.2.1. *Experiment 1.* This experiment analyzes the algorithm's performance with exponent p_1 under 10% Gaussian noise while varying the regularization parameter λ. We employ a uniform mesh with $h = 0.0086$ and set the tolerance to 1×10^{-6}.

Figure 6 displays the reconstruction results for $\lambda = 500, 1000$, and 10000. The left column shows the exact solution u_e, the center column the noisy data $f = u_e + \xi$, and the right column the denoised solution u_h. Figure 7 provides cross-sectional comparisons, demonstrating the algorithm's ability to recover smooth approximations across different λ values.

Table 3 details the convergence behavior for different λ values. We observe decrease in both the modular error and relative L^2 error across all cases. The gradient norm ratio shows oscillatory behavior for $\lambda = 500$ but converges in later iterations. For $\lambda = 1000$ and $\lambda = 10000$, we observe consistent monotonic decrease in the last iterations. The results demonstrate the significant impact of λ on both convergence behavior and reconstruction quality.

5.2.2. *Experiment 2.* In this experiment, we compare the behavior of Algorithm 4.1 (PDA) when facing increased amounts of Gaussian noise, considering two variable exponents and a

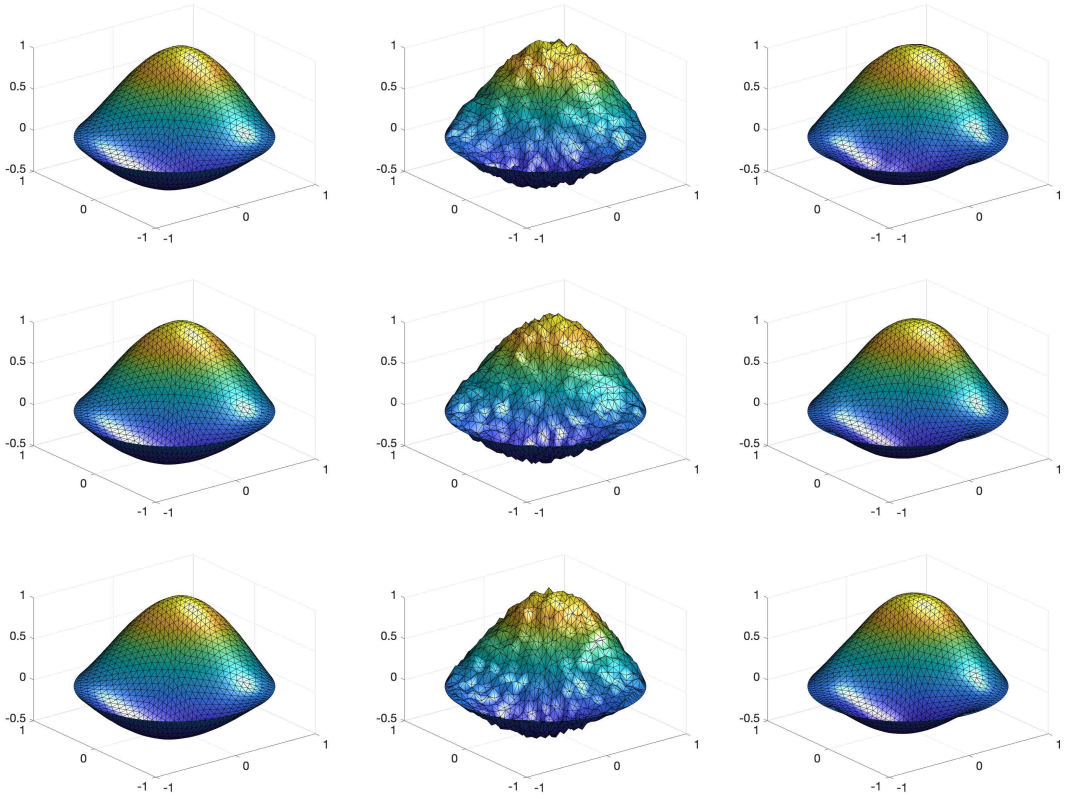

FIGURE 6. Experiment 1. u_e (left column), $u_e+\xi$ (central column) and u_h (right column), for $\lambda = 500$ (upper row), $\lambda = 1000$ (central row) and $\lambda = 10000$ (lower row). Parameters: $\xi = 10\%$

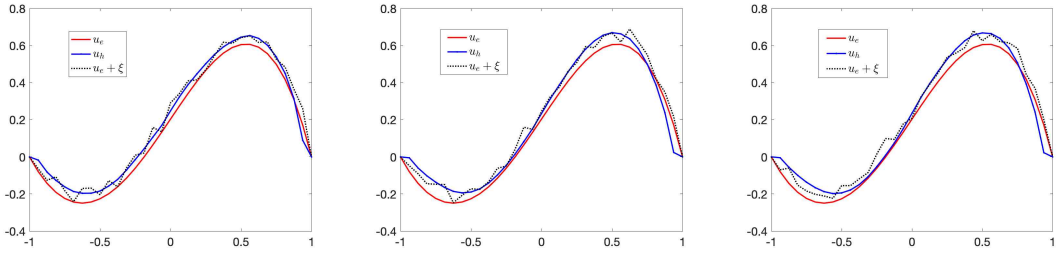

FIGURE 7. Experiment 1: Comparison between u_e, $u_e+\xi$ and u_h, with $\xi = 10\%$, for $\lambda = 500$ (left column), $\lambda = 1000$ (center column) and $\lambda = 10000$ (right column).

fixed value for the parameter $\lambda = 100$. We employ a uniform mesh with $h = 0.0086$ and we do not use the stopping criterion, but allow the algorithm to run for 40 iterations at each setting.

Figures 8 and 9 present the denoising results for p_1 and p_2, respectively. Each figure displays the noisy function $u_e+\xi$, the computed solution u_h, and cross-sectional profiles comparing u_e, u_h, and $u_e+\xi$ along a diameter of the domain. Images in the top, middle, and bottom rows contain 20%, 30% and 40% noise, respectively.

λ	# iter	$\int_\Omega \frac{1}{p(x)}\lvert\nabla(u_e-u)\rvert^{p(x)}\,dx$	err_u	$\frac{\lVert J'_{h,\mathscr{T}}(u_h^k)\rVert_{2,h}}{\lVert J'_{h,\mathscr{T}}(u_h^0)\rVert_{2,h}}$	$J_{h,\mathscr{T}}(u_h^k)$
	9	0.1810	0.1398	1.6606e-5	3.2742
	10	0.1655	0.1211	3.9143e-6	3.2265
	11	0.1692	0.1351	1.0783e-5	3.1911
500	12	0.1598	0.1223	1.2339e-6	3.1664
	13	0.1634	0.1332	7.4483e-6	3.1463
	14	0.1571	0.1232	2.9264e-7	3.1317
	1	1.1222	0.5275	0.0021	47.4899
	2	0.4835	0.2056	6.4562e-4	14.3642
	3	0.4092	0.2338	0.0183	8.3233
1000	4	0.2997	0.1383	0.0048	6.2831
	5	0.2805	0.1763	0.0010	5.2596
	6	0.2283	0.1299	3.4473e-7	4.6651
	1	1.1244	0.5295	2.1154e-4	457.9713
	2	0.4840	0.2027	6.6288e-5	118.7479
	3	0.4174	0.2373	0.0188	57.8648
1e4	4	0.3086	0.2413	0.0048	37.2822
	5	0.2917	0.1807	9.1902e-4	27.0607
	6	0.2396	0.1341	5.5923e-8	21.0634

TABLE 3. Convergence history for Experiment 1.

The results clearly demonstrate the algorithm's capability to recover smooth approximations of u_e from noisy data. As expected, increased noise levels present greater challenges for the reconstruction, yet the algorithm maintains effective noise suppression while preserving essential features of the original function. The pronounced smoothing effect observed in these experiments suggests that this algorithm could be advantageously incorporated into multigrid structures or similar multilevel approaches, where regularization of intermediate solutions plays a crucial role.

Table 4 summarizes the algorithm's performance after 40 iterations. Both modular errors and relative L^2 errors increase with noise level, as expected, while the gradient norms confirm convergence to stationary points. The consistent behavior across different exponents demonstrates the algorithm's robustness.

Figure 10 shows the monotonic convergence of the objective functional across all configurations, with values stabilizing within the 40 iterations. This convergence behavior, combined with the effective smoothing demonstrated in Figures 8 and 9, reinforces the algorithm's potential for integration into more sophisticated computational frameworks.

Finally, we note that a relatively low value of λ was employed in these experiments, as higher values tended to induce instability in the algorithm's performance. This observation motivates the development of an adaptive strategy for the functional parameter $\lambda(x)$, which could locally improve approximations across the domain. Such an approach will be investigated in future contributions.

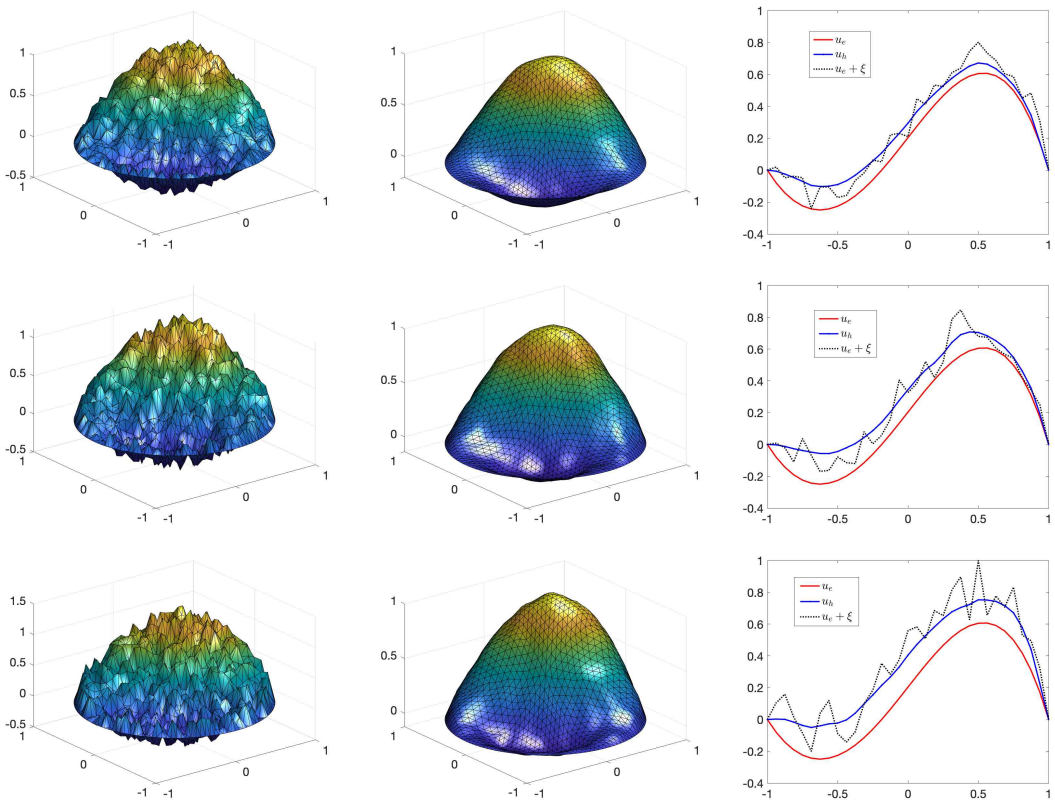

FIGURE 8. Experiment 2. $u_e+\xi$ (left column), u (right column) and the comparison between u_e, $u_e+\xi$ and u along the diameter of the domain, for $\xi = 20\%$ (upper row), $\xi = 30\%$ (middle row) and $\xi = 40\%$ (lower row). Variable exponente $p_1(x,y)$. Parameters: $\lambda = 100$.

$p(x)$	$\%\xi$	$\int_\Omega \frac{1}{p(x)}\lvert\nabla(u_e-u)\rvert^{p(x)}\,dx$	err_u	$\frac{\lVert J'_{h,\mathscr{T}}(u_h^k)\rVert_{2,h}}{\lVert J'_{h,\mathscr{T}}(u_h^0)\rVert_{2,h}}$	$J_{h,\mathscr{T}}(u_h^k)$
p_1	20%	0.2885	0.2482	8.5860e-7	3.0143
	30%	0.5457	0.3712	6.9781e-7	3.5059
	40%	0.7582	0.4661	2.6850e-6	4.2665
p_2	20%	0.4686	0.2594	1.7469e-6	3.0475
	30%	0.6901	0.3701	1.8417e-6	3.5530
	40%	1.1336	0.4999	3.3941e-6	4.1559

TABLE 4. Experiment 2: Estimators after 40 iterations of algorithm PDA.

6. CONCLUSIONS AND OUTLOOK

We analysed a class of optimization problems, involving the $p(x)$-Laplacian operator, which usually arise in the analysis of signals and imaging. We studied the well posedness of the problem in a suitable space with variable exponent, which provides a suitable framework for the analyzed problems, considering the local and the non-local behaviour of the involved functions. We developed a finite element discretization for the problem and extended the "frozen

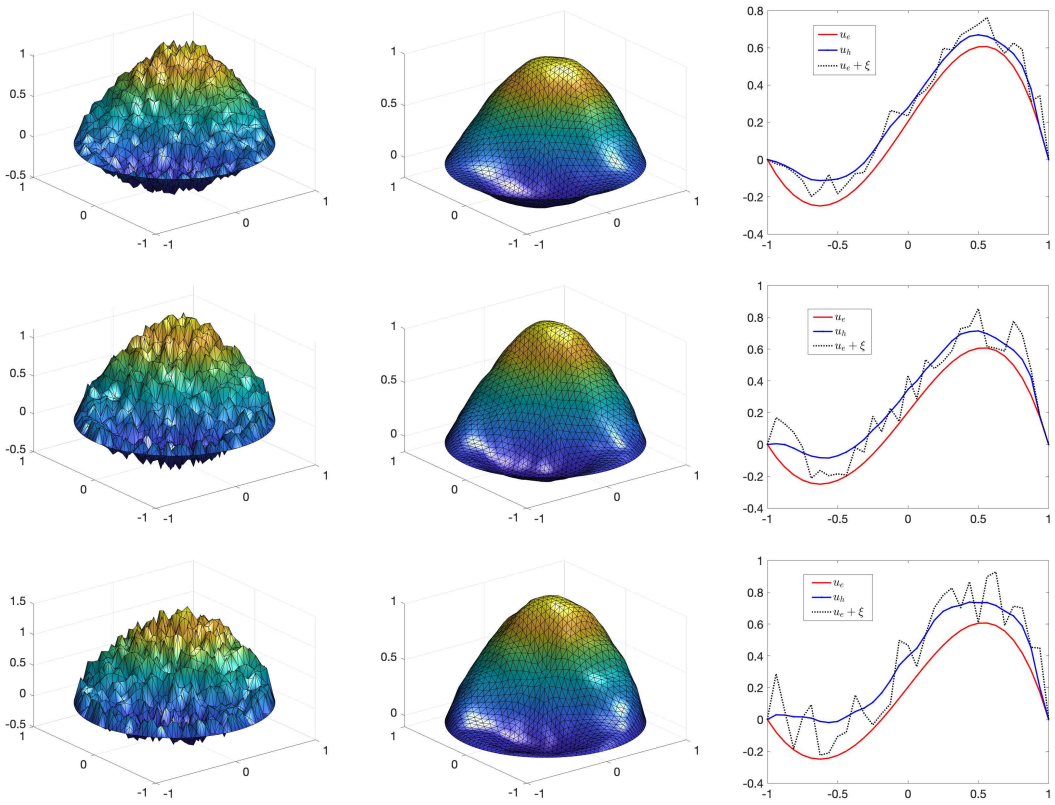

FIGURE 9. Experiment 2. $u_e+\xi$ (left column), u (right column) and the comparison between u_e, $u_e+\xi$ and u along the diameter of the domain, for $\xi = 20\%$ (upper row), $\xi = 30\%$ (middle row) and $\xi = 40\%$ (lower row) Variable exponente $p_2(x,y)$. Parameters: $\lambda = 100$.

exponents" approach to the discretized problem. Next, we proposed and implemented a preconditioned descent algorithm, based on the construction of preconditioned descent directions which are solutions of variational equations involving the frozen exponent modulars. Finally, we carried out three numerical experiments showing the main features of the algorithm.

In future contributions, we will focus on the application of the proposed methodology to imaging and denoising problems. Mainly, we are interested in the bilevel approach with a functional parameter λ. We also consider that the study of multigrid and multilevel type algorithms is a field worth to explore. The smoothing ability of the algorithm suggest to go this way. This work could be of great interest in the electrorheological fluids simulation, regarding the large-scale systems that usually arise when solving this kind of problems.

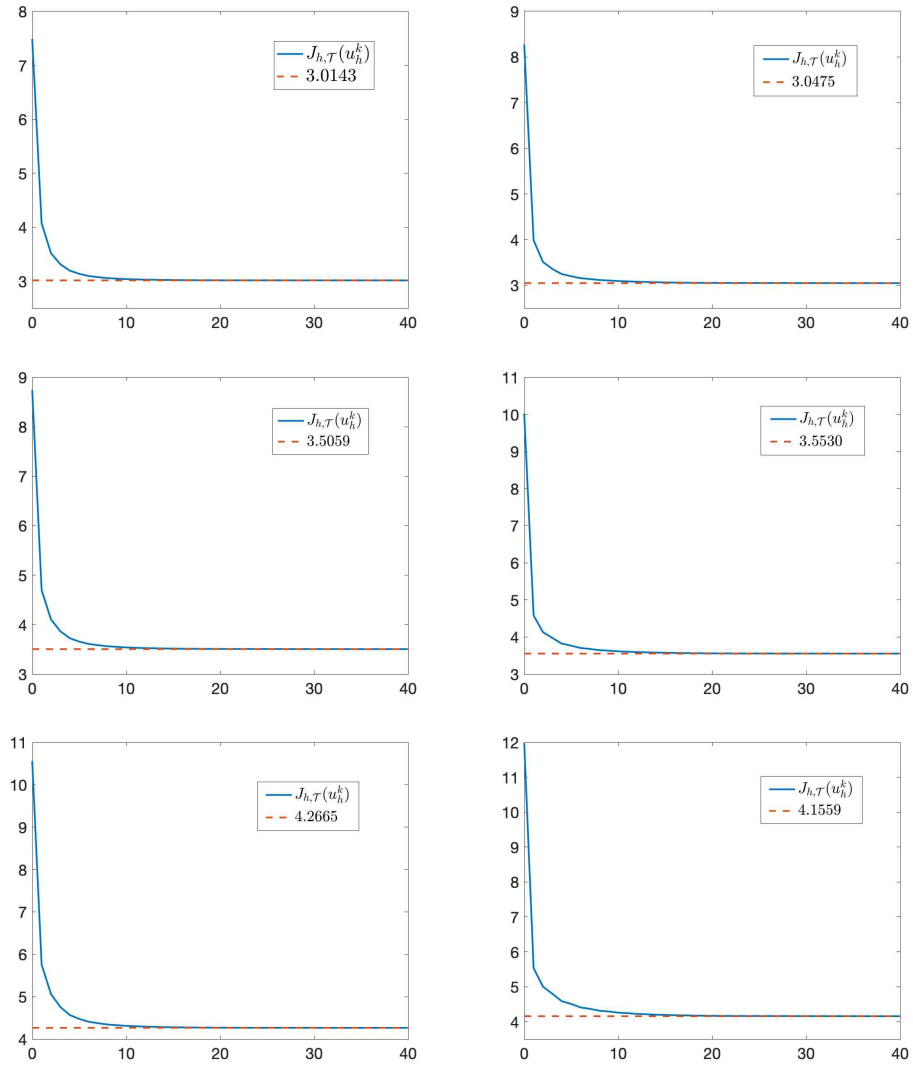

FIGURE 10. Experiment 2. Evolution of the objective functional for p_1 (left column) and p_2 (right column): $\xi = 20\%$ (upper row), $\xi = 30\%$ (middle row) and $\xi = 40\%$ (lower row). Parameters: $\lambda = 100$

REFERENCES

[1] G. Akagi, K. Matsuura, Nonlinear difussion equations driven by the $p(\cdot)$-Laplacian, Nonlinear Differ. Equ. Appl. 20 (2012), 37-64.

[2] M. Allaoui, A. El Amrouss, A. Ourraoui, Existence and uniqueness of solution for $p(x)$-Laplacian problems, Bol. Soc. Paran. Mat. 30 (2015), 225-232.

[3] E. M. Bollt, R. Chartrand, S. Esedoḡlu, P. Schultz, K. R. Vixie, Graduated adaptive image denoising: local compromise between total variation and isotropic diffusion, Adv. Comput. Math. 31 (2009), 61–85

[4] D. Breit, L. Diening, S. Schwarzacher, Finite element approximation of the $p(\cdot)$-Laplacian, SIAM J. Numer. Anal. 53 (2015), 551-572.

[5] S.S. Byun, J. Ok, On $W^{1,q(\cdot)}$-estimates for elliptic equations of $p(x)$-Laplacian type, J. Math. Pures Appl. 106 (2016) 512-545.

[6] M. Caliari, S. Zuccher, Quasi-Newton minimization for the $p(x)$-Laplacian problem, J. Comput. Appl. Math. 309 (2017), 122-131.

[7] M. Caliari, S. Zuccher, The inverse power method for the $p(x)$-Laplacian problem, SIAM J. Appl. Math. 66 (2006), 1383–1406.

[8] Y. Chen, S. Levine, M. Rao, Variable exponent, linear growth functionals in image restoration, J. Sci. Comput. 65 (2015), 698–714.

[9] L. Del Pezzo, A. L. Lombardi, S. Martínez, Interior penalty discontinuous Galerkin FEM for the $p(x)$-Laplacian, SIAM J. Numer. Anal. 50 (2012), 2497–2521.

[10] L. Del Pezzo, A. L. Lombardi, S. Martínez, Order of convergence of the finite element method for the p(x)-Laplacian, IMA J. Numer. Anal. 35 (2015), 1864–1887.

[11] J. E. Dennis, R. B. Schnabel, Numerical Methods for Unconstrained Optimization and NonlinearEquations, SIAM, Philadelphia, 1996.

[12] L. Diening, P. Harjulehto, P. Hästo, M. Růžička, Lebesgue and Sobolev Spaces with Variable Exponents, Springer, Verlag, Heidelberg, 2011.

[13] S. González-Andrade, A Preconditioned Descent Algorithm for Variational Inequalities of the Second Kind Involving the p-Laplacian Operator, Comput. Optim. Appl. 66 (2017), 123-162.

[14] S. González-Andrade, S. López-Ordóñez, A Multigrid Optimization Algorithm for the Numerical Solution of Quasilinear Variational Inequalities Involving the p-Laplacian, Comput. Math. Appl. 75 (2018), 1107-1127

[15] M. R. Grossinho, S. Agop Tersian, An Introduction to Minimax Theorems and Their Applications to Differential Equations, Springer, , 2001.

[16] Y. Q. Huang, Ruo Li, W. Liu, Preconditioned descent algorithms for p-Laplacian, J. Sci. Comput. 32 (2007), 343-371.

[17] P. S. Ilias, Dirichlet problem with $p(x)$-laplacian, Math. Reports, 10 (2008), 43–56.

[18] C.T. Kelley, Iterative Methods for Optimization, SIAM, Philadelphia, 1999.

[19] M. Růžička, Electrorheological Fluids: Modeling and Mathematical Theory, Springer, Berlin, 2000.

[20] F. Tröltzsch, Optimal Control of Partial Differential Equations. Theory, Methods and Applications, Amer. Math. Sco. 2010.